Layered microdomains and columnar grains in epitaxial $La_{0.7}Ca_{0.3}MnO_3$ films and $Y_{0.7}Ca_{0.3}MnO_3/La_{0.7}Ca_{0.3}MnO_3$ multilayers

C.J. Lu[a)] and Z.L. Wang[b)]
Beijing Laboratory of Electron Microscopy, Center of Condensed Matter Physics and Institute of Physics, Chinese Academy of Sciences, P.O. Box 2724, Beijing 100080, People's Republic of China

G.C. Xiong and G.J. Lian
National Mesocopic Physics State Key Laboratory and Department of Physics, Peking University, 100871 Beijing, People's Republic of China

Epitaxial $La_{0.7}Ca_{0.3}MnO_3$ thin film and $[Y_{0.7}Ca_{0.3}MnO_3/La_{0.7}Ca_{0.3}MnO_3]_{10}$ multilayers of about 140 nm in thickness were grown by pulsed laser deposition on $(001)LaAlO_3$. Their microstructures were investigated by transmission electron microscopy and associated techniques. It was found that both the film and the multilayers contain an almost defect-free layer near the substrate, followed by columnar grain grown. The columns were separated by strained regions in the top layer. No interfacial dislocations were observed at either of the $La_{0.7}Ca_{0.3}MnO_3/LaAlO_3$ or the $Y_{0.7}Ca_{0.3}MnO_3/La_{0.7}Ca_{0.3}MnO_3$ interfaces. Interestingly, both the epitaxial film and the multilayers exhibited layered crystallographic domains. The formation mechanisms of the layered domain structures observed are discussed.

I. INTRODUCTION

Recently, the observation of large magnetoresistance (MR) effects at room temperature in epitaxial $Ln_{1-x}A_xMnO_3$ (Ln = lathanides, A = alkaline earth elements or Pb) thin films has renewed interest in the doped manganite perovskite materials for potential magnetic random access memory and read-head applications.[1–4] However, a high magnetic field (several tesla) required for large MR still remains a barrier for any significant practical applications. Various efforts have been made to improve the low-field MR response of manganites. Such works include trilayer tunnel junctions,[5–7] polycrystalline thin films,[8–11] orthogonal grain chains,[12] artificially induced grain boundaries,[13,14] specially designed structures to focus the magnetic field,[15] etc. And it seems that introducing weak-link grain boundaries and interfaces is a promising way to enhance the low-field MR response in manganite films.

It has been shown that, in bulk materials, the Curie temperature T_c and MR in high magnetic fields are extremely sensitive to chemical pressure and hydrostatic pressure.[16,17] Several groups have reported that lattice strain affects the peak resistance temperature T_p and MR

properties of $La_{0.7}Sr_{0.3}MnO_3$ (LSMO),[18] $La_{0.7}Ca_{0.3}MnO_3$ (LCMO),[19] and $La_{0.8}Ca_{0.2}MnO_3$,[20] thin films, and the strain-induced magnetoelastic interaction plays a dominant role in the magnetic anisotropy.[18,4,21] Wang *et al.*[22] reported that large low-field MR had been obtained in compressively strained $Pr_{0.67}Sr_{0.33}MnO_3$ (PSMO) ultra-thin (<10 nm) films and found very different effects of compressive and tensile strain on the magnetic and the low-field MR properties.[23] These results demonstrate that lattice distortions in manganite films can dramatically alter their physical properties. Recently, we obtained large low-field MR in heteroepitaxial ferromagnetic/paramagnetic $Gd_{0.7}Ca_{0.3}MnO_3/La_{0.7}Ca_{0.3}MnO_3$ (GCMO/LCMO) multilayers and found that the transport properties and MR behavior of the multilayers are similar to those of ultrathin PSMO films.[24] In the multilayers, strain exists because of the difference in radii of La^{3+} and Gd^{3+} ions. However, the mechanism based on strain alone may not be sufficient to account for all aspects of the experimental results such as the thickness and temperature dependencies of the magnetic and low-field MR properties.[22–26] Other factors such as structural defects and spin disorder must also be considered in order to analyze quantitatively the magnetic and MR properties of the films and multilayers. In fact, crystallographic domain orientation can also play an important role in determining magnetic anisotropy.[25–27] Therefore, the characterization of microstructures, such as grain boundaries and crystallographic domain structures, is important

for studying magnetism, particularly magnetic anisotrophy and low-field MR response, in these films and multilayers.

In the multilayers, there are interfaces composed of two different materials, which provide a good opportunity to study the coupling, interaction, proximity, and the effect of strain, *etc.,* across the interfaces between these materials. Compared to those on a single magnetic layer, however, there are relatively few studies on doped manganite-based multilayers showing enhanced MR.[24,28–32] In this study, heteroepitaxial $Y_{0.7}Ca_{0.3}MnO_3/La_{0.7}Ca_{0.3}MnO_3$ (YCMO/LCMO) multilayers have been fabricated by pulsed laser deposition (PLD) and their microstructures investigated by transmission electron microscopy (TEM) and associated techniques. It is well-known that YCMO is a paramagnetic insulator like GCMO. It is expected that the LCMO layers in the multilayers would be under a compressive stress because the radius of Y^{3+} ions is smaller than that of La^{3+}. For ease of comparison, LCMO thin films have also been prepared under the same deposition conditions and their microstructure has been investigated.

II. EXPERIMENTAL

Epitaxial LCMO thin film and $[YCMO/LCMO]_{10}$ multilayers of approximately 140 nm in thickness were grown on (001) $LaAlO_3$ (LAO) substrates by PLD. The PLD system and deposition processes have been described previously.[33] Sintered ceramic targets with nominal compositions of $La_{0.7}Ca_{0.3}MnO_3$ and $Y_{0.7}Ca_{0.3}MnO_3$ were used alternatively for preparing multilayers. In multilayer deposition, the targets were changed *in situ* as required and given laser pulses were controlled with a computer. The substrate temperature was 750 °C during deposition. The oxygen pressure during deposition was kept at 25 Pa. After deposition the as-grown films were directly cooled to room temperature in O_2. No further thermal treatment was performed on the samples after deposition. For the convenience of comparison, the LCMO film was prepared under the same experimental conditions as the multilayers. The resistance measurements were performed in a four-point geometry in a temperature range 20–300 K.

The YCMO/LCMO multilayers and LCMO thin film were examined by TEM in cross-sectional view. The cross-sectional slices for TEM investigation were obtained by cutting the LCMO/LAO and [YCMO/LCMO]$_{10}$/LAO samples along the [100] direction of LAO and then gluing the cut slides face-to-face by joining the surfaces of the film or multilayers. TEM specimens were prepared by mechanical grinding, polishing, and dimpling, followed by Ar-ion milling at 4.5 kV. Selected area diffraction (SAED) patterns, high-resolution electron microscopy (HREM) images, and

electron energy loss spectrum (EELS) spectra were recorded in a Philips CM200/FEG (Eindhoven, The Netherlands) transmission electron microscope equipped with a Gatan (Gatan, Inc., Pleasanton, CA) imaging filter. Element maps were created using the Gantan digital micrograph software.

III. STRUCTURAL CONSIDERATIONS

$La_{0.7}Ca_{0.3}MnO_3$ is a distorted perovskite with a pseudocubic lattice parameter of $a_c = 0.3858$ nm. The tilting of MnO_6 octahedra results in an orthorhombic structure with the space group of *Pnma* and the lattice parameters of $a \approx b \approx \sqrt{2}a_c$ and $c = 2a_c$.[34] In this work, indexing is generally based on the orthorhombic unit cell, except in certain cases where the subscript "c" is used to refer to the pseudocubic unit cell. The LAO substrate also has a perovskite structure with a slight rhombohedral distortion ($a = 0.3788$ nm, $\alpha = 90° \, 4'$) at room temperature. LAO experiences a structural phase transition from a rhombohedral to a cubic structure ($a = 0.381$ nm) on heating to $T_c = 435$ °C.[35] When LCMO grows epitaxially on (001) LAO substrates, six possible domain orientations can exist in a LCMO thin film, as shown schematically in Fig. 1. For clarity, the pseudocubic perovskite unit cell of LCMO is shown in the figure with orthorhombic indexing of the unit cell directions. The six possible orientation relationships between the LCMO film and substrates can be described as:

Type X: LCMO(110)[001]//LAO(001)[100] ;

Type X': LCMO($1\bar{1}0$)[001]//LAO(001)[100] ;

Type Y: LCMO(110)[001]//LAO(001)[010] ;

Type Y': LCMO($1\bar{1}0$)[001]//LAO(001)[010] ;

Type Z': LCMO(001)[$1\bar{1}0$]//LAO(001)[010] .

Among the six types of domains in LCMO, X(X'), Y(Y'), and Z(Z') type domains can be distinguished by means of TEM, while the difference between the X (Y or
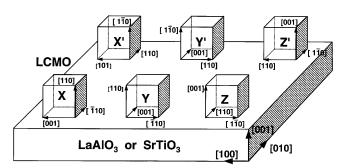

FIG. 1. Schematic diagram showing six possible orientations of epitaxial LCMO (or YCMO) layers grown on (001) LAO substrates (After Jiang *et al.*[36]). Note that while the pseudocubic perovskite unit cell of LMCO is drawn, the cell directions are indexed on the basis of the orthorhombic unit cell.

Z) and X′ (Y′ or Z′) is not distinguishable by the same technique due to the pseudocubic character of the LCMO structure. In the present work, we only classify the domains as three types (X, Y, and Z). In fact, the three types of domain orientations correspond to three possible *c*-axis directions of the orthorhombic LCMO, i.e., the *c*-axis of LCMO is parallel to the [100], [010], or [001] direction of the substrate, respectively. The domains with X- or Y-type orientation relationships are called [110] oriented and those with Z-type [001] oriented, since their [110] and [001] axes are perpendicular to the substrate surface, respectively.

YCMO has the same space group as LCMO, and its lattice parameters are very close to those of LCMO. Thus, YCMO layers also can exhibit the six possible orientations shown in Fig. 1 when they grow on LAO.

Because of the systematic absence of (00*n*) (*n* = odd integer) and the degeneracy of d_{110} and d_{002} spacing the orthorhombic LCMO, it is impossible to distinguish the [110] or [001] orientations from normal XRD θ–2θ scans. This ambiguity can be easily resolved by using electron diffraction. Figure 2 shows the schematic electron diffraction patterns of LCMO or (YCMO) in <001> and <110> directions. Except the differences due to the weak reflections, the patterns in Fig. 2 are identical. The {111} and {100} reflections, which are very weak in x-ray diffraction (<1%), appear in electron diffraction patterns with considerable intensities due to dynamic scattering effects. The forbidden reflections, such as {001}, {003}, and {110}, also appear in the patterns in Figs. 2(b) and 2(c) for relative thick samples due to dynamic double diffraction. The orientation of the [001] axis can be easily determined on the basis of the relationship shown in Fig. 2. The pattern of Fig. 2(a) corresponds to a film with [001] axis parallel to the electron beam. The patterns in Figs. 2(b) and 2(c), on the other hand, indicate that the [001] axis is in a direction perpendicular to the electron beam.

IV. RESULTS

A. LCMO film

The epitaxial LCMO thin film exhibits the semiconducting–metallic transition at T_p = 262 K with MR behavior. The T_p of the film is very close to that for

bulk LCMO (265 K). Figure 3 shows the temperature dependence of the resistivity for the LCMO film at zero field. A rapid drop in electric resistivity can be seen below 260 K. The lower residual resistivity (<1 mΩ cm) at 20 K emphasizes a good metallic behavior. A ferromagnetic transition was really observed in the magnetization measurement for the LCMO film. MR behavior was also observed by applying magnetic fields.

Figure 4(a) shows a low magnification TEM bright-field image showing the cross-sectional morphology of the LCMO film on LAO. The film has a rough surface and a sharp interface with the substrate. The average thickness of the film is about 140 nm, and the surface roughness is approximately 15 nm. The layered structure can be clearly seen from Fig. 4(a). The pattern of diffuse bright line segments normal to the interface reveals the columnar grain growth which occurs in a band parallel to the interface after a thickness of approximately 50 nm. Between this band and the substrate surface a featureless LCMO layer is present, as indicated by an arrowhead, suggesting that the initial 50-nm layer is almost perfect crystalline. At this time the origin of the layered growth of the LCMO thin films is still unclear, but it is interesting to compare our results with those published previously. Lebedev *et al.*[37] reported that very thin (approximately 20 nm) LSMO films exhibit a perfect monocrystalline structure, while thicker films (approximately 70 nm) show the presence of a columnar structure. Lebedev *et al.*[34] also reported that, at the deposition temperature of 800°C, a perfectly monocrystalline layer with a thickness of about 50 nm, separating the substrate and the columnar structure, is formed in the PLD-deposited LCMO/STO thin films. Clearly, their reports are consistent with our observation. On the other hand, Gommert *et al.*[38] reported that on-axis-deposited LCMO thicker films were found to grow with a large number of defects, whereas off-axis prepared samples develop a columnar microstructure. In contrast to Gommert *et al.*'s report, our LCMO film was on-axis deposited. The resistivities of the epitaxial LCMO thin films of different thickness were measured. It was found that the resistivities of the films decreased as the film thickness increased. This indicates that the top columnar layer shows lower resistivity than the almost defect-free LCMO layer close to the substrate.
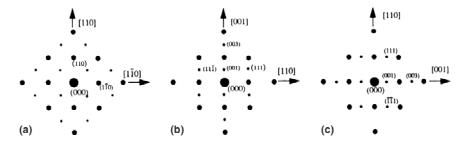

FIG. 2. Schematic electron diffraction patterns of LCMO (or YCMO) in the (a) <001> and (b,c) <110> directions.

Figures 4(c) and 4(d) show SAED patterns taken from the top layer and an area including both the film and the substrate, respectively. The pattern of Fig. 4(c) is a [1$\bar{1}$0] zone electron diffraction pattern of the orthorhombic LCMO. The pattern in Fig. 4(d) is indexed on the basis of the pseudocubic unit cell and consists of at least three patterns of the orthorhombic LCMO superimposed. Figure 4(b) shows a cross-sectional TEM dark-field image obtained by using the weak reflection marked by "Z" from Fig. 4(c). A clear interface can be seen in the film at a height of about 50 nm. The top layer above the interface shows bright, whereas the bottom layer below it is gray. These indicate that mixed domains of [110] and [001] orientations are present in the film with three *c*-axis directions. The top layer with a thickness of approximately 100 nm is almost pure [001] oriented with the *c*-axis perpendicular to the substrate surface, but the layer between the top LCMO and the substrate exhibit an almost pure [110] out-of-plane texture with 90° domains in plane. Figure 5 is a typical cross-sectional HREM image of the LCMO/LAO interface. The interface is atomically sharp without chemical reaction, and the contact plane is a common La(Ca) layer. No interfacial dislocations were observed at/near the interface.
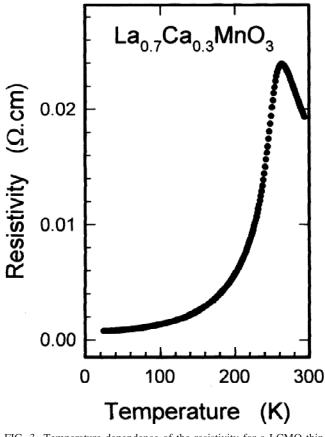

FIG. 3. Temperature dependence of the resistivity for a LCMO thin film in zero magnetic field.

B. YCMO/LCMO multilayers

Figures 6(a) and 6(b) present two low-magnification cross-sectional TEM bright-field images of [YCMO/LCMO]$_{10}$/LAO multilayers, which show the columnar structure and layered structure of the multilayers, respec-
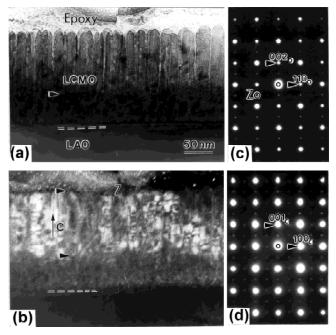

FIG. 4. (a) Cross-sectional TEM bright-field image of LCMO thin film grown on LAO showing columnar grain growth and the layered domain structure, along with SAED patterns taken from (c) the top layer and (d) an area including both film and substrate. Pattern (c) is indexed on the basis of the orthorhombic LCMO, while (d) on the single perovskite unit cell. (b) Cross-sectional TEM dark-field image obtained using the weak reflection Z in (c). The arrow denotes the *c*-axis direction of the top layer.
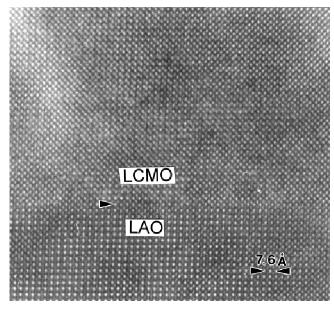

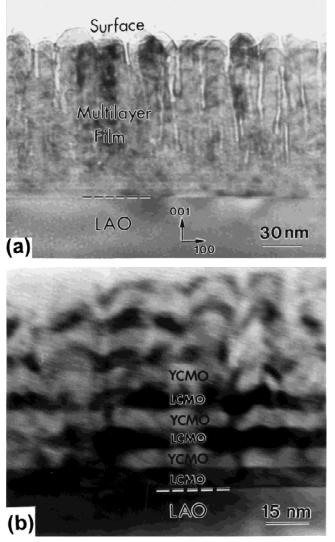FIG. 5. Cross-sectional HREM image of the LCMO film on LAO.

FIG. 6. Low-magnification cross-sectional TEM bright-field images of [YCMO/LCMO]$_{10}$/LAO multilayers showing (a) columnar grains and (b) layered structure.

tively. In a similar manner to the LCMO film, columnar grains in the multilayers are separated by strained regions which start at a height of around 30–50 nm. It can be seen from Fig. 6(a) that the surface of the multilayers is rough due to the columnar-grain growth. The average diameter of the columnar grains is about 15 nm, and the surface roughness is approximately 15 nm. The thickness of the whole multilayer structure is about 140 nm, and each layer is approximately 7 nm thick. Interestingly enough, one can clearly see the contrast difference between LCMO and YCMO layers in the bright-field image of Fig. 6(b), probably as a result of atomic number effect on scattering absorption etc. The YCMO/LCMO interfaces near the LAO substrate also show a little roughness, indicating that the multilayers nucleated and grew according to the island growth model, at least during the early stages of deposition.

Figures 7(a) and 7(b) show SAED patterns taken from the cross-sectional YCMO/LCMO multilayers and LAO substrate, respectively. By comparison of the two patterns, it can be drawn that the multilayers are heteroepitaxially grown on LAO. The pattern in Fig. 7(a) is indexed on the basis of the pseudocubic unit cell, and it consists of at least the [001] and [110] zone patterns of the orthorhombic LCMO and/or YCMO (see Fig. 2). Figures 7(c) and 7(d) are dark-field images obtained by using weak reflections Y and X from Fig. 7(a), respectively. Arrows denote the *c*-axis directions of bright layers. More interestingly, LCMO layers are generally bright in Fig. 7(c) while YCMO layers are bright in Fig. 7(d). This indicates that the multilayers exhibit an almost pure [110] out-of-plane texture with 90° domains in plane. Almost all LCMO layers are of Y-type domain orientations, while YCMO layers of X-type. It is also of interest to note that almost all columnar grain boundaries are dark in both Figs. 7(c) and 7(d), suggesting that the boundaries are not of the orthorhombic structure due to the large strain.

Figure 8 shows a cross-sectional HREM image of the YCMO/LCMO multilayers. Note that YCMO layers show a clear doubling periodicity in one [MnO$_2$] layer out of two along their *c*-axis direction, whereas a cubic-like structure with *c*-axis in the line of sight can be seen from the LCMO layers. The interfaces are atomically sharp without chemical reaction. No interfacial dislocations were observed at either the LCMO/LAO interface or YCMO/LCMO interfaces. It is interesting to study the local strain field of individual layers. To measure the tetragonal deformation of perovskite unit cells, the inter-dot spacings were measured by means of photometry plots of HREM dot images along both a normal to an interfaces and a direction parallel to that interface. Fifteen dot spacings along the two directions were measured at different layers. It is found that the tetragonal deformation *c/a* (*a* and *c* refer to the out-of-plane and in-plane lattice parameters, respectively) of the second LCMO and YCMO layers (number from the substrate surface) are about 1.022 and 0.9925, respectively. This indicates that the LCMO and YCMO layers are elastically strained in opposite senses such that the interfaces between them are perfectly coherent. There is no difference between the lattice parameters parallel to the interfaces. Close to the multilayer–substrate interface, both the first LCMO layer and LAO surface layer are also elastically strained in opposite senses such that the interface is perfectly coherent. Similar elastic strain behavior also was found at LSMO/LAO film–substrate interfaces by Lebedev *et al.*[37]

Figure 9 shows an EELS spectrum obtained from the YCMO/LCMO multilayers, where the Y–M$_3$, Ca–L$_{2,3}$, O–K, Mn–L$_{2,3}$, and La–M$_{4,5}$ edges are in the displayed energy loss region. The fine structures of O–K or Mn–L$_{2,3}$ edges are inserted. The three fine peaks observed in the
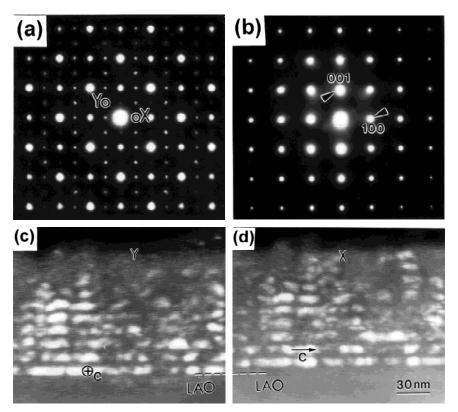
FIG. 7. SAED patterns taken from (a) the cross-sectional YCMO/LCMO multilayers and (b) LAO substrate. (c) and (d) are dark-field images obtained by using weak reflections Y and X from (a), respectively. Arrows denote the c-axis directions of bright layers, and a ring with a cross in it shows the end of an arrow normal to the image.

O–K edge indicate three valence states located below the edge of the conduction band. Figure 10 shows an element map of the YCMO/LCMO multilayers for the La–$M_{4,5}$ edge. The image clearly shows the distribution of the thickness integrated La concentration, and the YCMO/LCMO interface is reasonably sharp, although the signal-noise ratio is poor due to low signal intensity at this high energy loss region. The image shows that the YCMO/LCMO interface is chemically sharp and that interdiffusion, if it exists, is limited to one to two atomic layers. Also, there can be no significant substitution between Y^{3+} and La^{3+} ions at columnar grain boundaries.

V. DISCUSSION

A. About the formation mechanism of layered domains in LCMO film

The LCMO film on LAO was observed to have a layered domain structure, with a [110] texture layer close to the substrate, followed by [001] oriented domains at a higher thickness. Lu *et al.*[39] reported similar layered domain structure in $SrRuO_3$ thin films deposited by PLD on $(001)SrTiO_3$ (STO), i.e., [110] oriented domains with a thickness of approximately 25 nm close to the substrate, followed by [001] oriented domains with

increasing thickness. In fact, $SrRuO_3$ has the same Gd–FeO_3-type structure as LCMO and the lattice mismatch for the $SrRuO_3$/STO system (−0.5%) is similar to that for our LCMO/LAO (−1.7%). Considering the ortho-rhombic LCMO as a pseudocubic structure, the crystallographic axes for the cell, a_c, b_c, and c_c, are 1/2[110], 1/2[1$\bar{1}$0], and 1/2[001], respectively. Because the pseudocubic parameters are essentially identical in the magnitude, it would be difficult to understand why the [110] orientations should grow initially on LAO if only considering the lattice parameter match between the film and substrate.

It may be noted that the angle between 1/2[110] and 1/2[1$\bar{1}$0] of the LCMO is 90.04° while the angle between both these vectors and 1/2[001] is 90°. As has previously been discussed[40], the domains in LCMO films are not necessarily formed during film growth. Distorted (ortho-rhombic) perovskites usually undergo a phase transition to a more symmetric structure at elevated temperature. For bulk LCMO, differential thermal analysis data indicates a phase transition around 500 °C,[41] which makes it likely that, for films as well as bulk material, the structure at the growth temperature is different from the one at low temperature. In such a case, the domains could be formed during cooling of the sample. Therefore, the columnar structure formed in the top layer may play an important

role in the formation of the domain structures. It should also be noted that the LCMO films are grown above the T_c of the substrate LAO (435 °C), whereas the structural studies are performed at room temperature, i.e., below
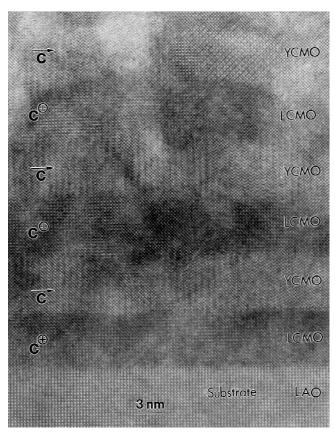
the T_c. The symmetry breaking at the phase transition gives rise to twin structures in the low-temperature phase of LAO.

At this time, the formation mechanism of the observed domain structure in our LCMO film is not yet completely clear. However, it is interesting to compare our results with previous reports. On the basis of grazing incidence XRD experiments, Rao *et al.*[20] studied the evolution of crystallographic domain orientations of $La_{0.8}Ca_{0.2}MnO_3$ films grown by PLD on LAO and STO as a function of film thickness. It was found that very thin (<25 nm) films grown on LAO exhibited a pure [110] out-of-plane texture with 90° domains in plane, while films on STO showed a single [001] orientation. As film thickness increased, the pure domain orientations were replaced by mixed ones, where both [001] and [110] oriented domains coexisted, with the degree of mixing increasing with thickness. The observed strain state and domain structure were strongly correlated with each other, indicating that they were linked directly. For instance, the rapid in-plane lattice relaxation in $La_{0.8}Ca_{0.2}MnO_3$ films on STO seemed to be associated with the initial appearance of [110] texture. Similarly, the formation of [001] oriented domain on the top layer of our LCMO film may be related to the almost complete in-plane relaxation due to the presence of numerous columnar-grain boundaries after a thickness of approximately 50 nm. We examined a 150-nm-thick LCMO epitaxial film grown also by PLD on LAO.[40] In contrast to the LCMO film in this present study, the LCMO film reported in Ref. 40 did not show any columnar structure and exhibited an almost pure [110] texture, which may be caused by a large residual in-plane compressive stress.
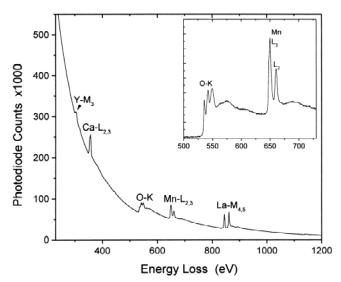

FIG. 8. Cross-sectional HREM image of YCMO/LCMO multilayers on LAO substrate. Arrows indicate the *c*-axis directions from layer to layer.

FIG. 9. EELS spectrum obtained from YCMO/LCMO multilayers. The inset shows the corresponding EELS spectrum of O-K and Mn-$L_{2,3}$ edges.
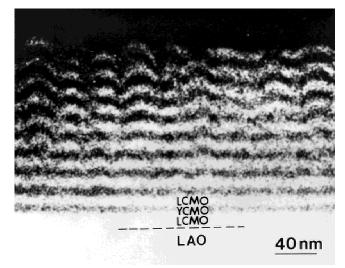

FIG. 10. Element map for La-$M_{4,5}$ edge of a YCMO/LCMO multilayer revealing the La distribution in the multilayer. Energy-window width: 20 eV.

B. About the formation mechanism of layered domains in multilayers

It has been found that the entire YCMO/LCMO multilayers exhibit an almost pure [110] out-of-plane texture. More interestingly, almost all LCMO layers are Y-type oriented while YCMO layers X-type. No interfacial dislocations were observed at either the LCMO/LAO interface or YCMO/LCMO interfaces. The LCMO and YCMO layers are elastically strained in opposite sense such that the interfaces between them are perfectly coherent. Since the La^{3+} ion is larger than the Y^{3+} ion, the lattice parameter of LCMO is larger than that of YCMO, and the lattice parameter of LCMO is also larger than that of LAO. Considering the ultralow thickness of each layer, it is to be expected that all the LCMO layers would be under an in-plane compressive stress and that the YCMO layers would be under a tensile stress, as has been observed in our HREM images. The [110] orientation of LCMO layers may be caused by such a large residual in-plane compressive stress. In contrast to the LCMO film, no [001] oriented top layer appears in these multilayers.

It has previously been found that very thin (<25 nm) LCMO films grown on STO show a single [001] orientation and that they are in tensile strain.[20,26] However, all YCMO layers are [110] oriented. Clearly, it would be difficult to understand the orientations of LCMO and YCMO layers if only their strain state is considered. In fact, the orientation domain formation can be very complex. At this time, we do not know the temperature at which YCMO experiences a transition from a simple perovskite to a distorted perovskite structure. Previous reports indicated that misorientation of the substrate is responsible for the formation of single crystalline films.[36,42] For our YCMO/LCMO multilayers containing columnar grains, it can be predicted that surface and interface properites, such as the orientation of the substrate, roughness, steps, kinks, and even surface reconstruction, may play an important role in formation of the orientation domains.

VI. CONCLUSIONS

Epitaxial LCMO thin film and [YCMO/LCMO]$_{10}$ multilayers were grown by PLD on (001) LAO. Their microstructures have been investigated by TEM and associated techniques. It was found that both the film and the multilayers contain an almost defect-free layer near the substrates, followed by columnar-grain growth. Columns are separated by strain regions in the top layer. No interfacial dislocations were observed at either the LCMO/LAO interface or YCMO/LCMO interfaces. The LCMO and YCMO layers are elastically strained in the opposite senses such that the interfaces between them are perfectly coherent.

It was also found that both the film and the multilayers show layered crystallographic domain structures. Mixed domains of [110] and [001] orientations are present in the LCMO film. The top layer is almost pure [001] oriented, whereas the layer between the top LCMO and substrate exhibits an almost pure [110] out-of-plane texture with 90° domains in plane. In contrast to the LCMO film, the [YCMO/LCMO]$_{10}$/LAO multilayers exhibit an almost pure [110] texture. In general, all LCMO layers are Y-type oriented whereas YCMO layers X-type. The formation mechanisms of the crystallographic domains observed in both the films and the multilayers have been discussed.

REFERENCES

1. P.B. Tavares, V.S. Amaral, J.P. Araujo, J.B. Sousa, A.A.C.S. Lourenco, and J.M. Vieira, J. Appl. Phys. **85,** 5411 (1999).
2. K.A. Thomas, P.S.I.P.N. de Silva, J.F. Cohen, A. Hossain, M. Rajeswari, T. Venkatesan, R. Hishes, and J.L. MacManus-Driscoll, J. Appl. Phys. **84,** 3939 (1998).
3. E.S. Vlakhov, R.A. Chakalov, R.I. Chakalova, K.A. Nenkov, K. Dorr, A. Handstein, and K.-H. Muller, J. Appl. Phys. **83,** 2152 (1998).
4. Y. Suzuki, H.Y. Hwang, S.-W. Cheong, and R.B. van Dover, Appl. Phys. Lett. **71,** 140 (1997).
5. J.Z. Sun, W.J. Gallagher, P.R. Duncombe, L. Krusin-Elbaum, R.A. Altman, A. Gupta, Y. Lu, G.Q. Gong, and G. Xiao, Appl. Phys. Lett. **69,** 3266 (1996).
6. Yu Lu, X.W. Li, G.Q. Gong, G. Xiao, A. Gupta, P. Lecoeur, J.Z. Sun, Y.Y. Wang, and V.P. Dravid, Phys. Rev. B **54,** R8357 (1996).
7. C. Kwon, Q.X. Jia, Y. Fan, M.F. Hundley, D.W. Reagor, J.Y. Coulter, and D.E. Peterson, Appl. Phys. Lett. **72,** 486 (1998).
8. A. Gupta, G.Q. Gong, G. Xiao, P.R. Duncombe, P. Lecoeur, P. Trouilloud, Y.Y. Wang, V.P. Dravid, and J.Z. Sun, Phys. Rev. B **54,** R15629 (1996).
9. X.W. Li, A. Gupta, G. Xiao, and G.Q. Gong, Appl. Phys. Lett. **71,** 1124 (1997).
10. R. Shreekala, M. Rajeswari, K. Ghosh, A. Goyal, J.Y. Gu, C. Kwon, Z. Trajanovic, T. Boettcher, R.L. Greene, R. Ramesh, and T. Venkateson, Appl. Phys. Lett. **71,** 282 (1997).
11. T. Walter, K. Dörr, K.-H. Müller, B. Holzapfel, D. Eckert, M. Wolf, D. Schläfer, L. Schultz, R. and Grötzschel, Appl. Phys. Lett. **74,** 2218 (1999).
12. H.B. Peng, B.R. Zhao, Z. Xie, Y. Lin, B.Y. Zhu, Z. Hao, Y.M. Ni, H.J. Tao, X.L. Dong, and B. Xu, Appl. Phys. Lett. **74,** 1606 (1999).

13. N.D. Mathur, G. Burnell, S.P. Isaac, T.J. Jackson, B.-S. Teo, J.L. MacManus-Driscoll, L.F. Cohen, J.E. Evetts, and M.G. Blamire, Nature **387,** 266 (1997).
14. C. Srinitiwarawong and M. Ziese, Appl. Phys. Lett. **73,** 1140 (1998).
15. H.Y. Wang, S-W. Cheong, and B. Batlogg, Appl. Phys. Lett. **68,** 3494 (1996).
16. H.Y. Hwang, S.W. Cheong, P.G. Radaelli, M. Marezio, and B. Batlogg, Phys. Rev. Lett. **75,** 914 (1995).
17. M.R. Ibarra, P.A. Algarabel, C. Marquina, J. Basco, and J. Garcia, Phys. Rev. Lett. **75,** 3541 (1995).
18. C.K. Kown, M.C. Robson, K.-C. Kim, J.Y. Gu, S.E. Lofland, S.M. Bhagat, Z. Trajanovic, M. Rajeswari, T. Venkatesan, A.R. Kratz, R.D. Gomez, and R. Ramesh, J. Magn. Magn. Mater. **172,** 229 (1997).
19. T.Y. Koo, S.H. Park, K.B. Lee, and Y.H. Jeong, Appl. Phys. Lett. **71,** 977 (1997).
20. R.A. Rao, D. Lavric, T.K. Nath, C.B. Eom, L. Wu, and F. Tsui, Appl. Phys. Lett. **73,** 3294 (1998).
21. J. O'Donnell, M.S. Rzchowski, J.N. Eckstein, and I. Bozovic, Appl. Phys. Lett. **72,** 1775 (1998).
22. H.S. Wang and Q. Li, Appl. Phys. Lett. **73,** 2360 (1998).
23. H.S. Wang, Q. Li, K. Liu, and C.L. Chien, Appl. Phys. Lett. **74,** 2212 (1999).
24. G.J. Lian, Z.H. Wang, J. Gao, J.K. Kang, M.Y. Li, and G.C. Xiong, J. Phys. D: Appl. Phys. **32,** 90 (1999).
25. H.S. Wang, Q. Li, K. Liu, and C.L. Chen, Appl. Phys. Lett. **74,** 2212 (1999).
26. J. Aarts, S. Freisem, R. Hendrikx, and H.W. Zandbergern, Appl. Phys. Lett. **72,** 2975 (1998).
27. M. Benaissa, K.M. Krishnan, E.E. Fullerton, and J.S. Jiang, IEEE Trans. Magn. **34,** 1204 (1998).
28. G.Q. Gong, A. Gupta, G. Xiao, P. Lecoeur, and T.R. McGuire, Phys. Rev. B **54,** R3742 (1996).
29. C. Kwon, K-C. Kim, M.C. Robson, J.Y. Gu, M. Rajeswari, and T. Venkatesan, J. Appl. Phys. **81,** 4950 (1997).
30. M. Sahana, M.S. Hegde, V. Prasad, and S.V. Subramanyam, J. Appl. Phys. **85,** 1058 (1999).
31. G.C. Xiong, Z.H. Wang, G.J. Lian, D.S. Dai, and Z.Z. Gan, J. Phys.: Condens. Matter **11,** 3187 (1999).
32. S. Sundar Manoharan, K.M. Satyalasksmi, V. Prasad, S.V. Subramanyam, and M.S. Hegde, Curr. Sci. **69,** 356 (1995).
33. G.C. Xiong, Q. Li, H.L. Ju, X.X. Xi, R.L. Greene, and T. Venkatesan, Appl. Phys. Lett. **66,** 1427 (1995).
34. O.I. Lebedev, G. Van Tendeloo, S. Amelinckx, B. Leibold, and H-U. Habermeier, Phys. Rev. B **58,** 8065 (1998).
35. S. Geller and V.B. Bala, Acta Crystallogr. **9,** 1019 (1956).
36. J.C. Jiang, W. Tian, X.Q. Pan, Q. Gan, and C.B. Eom, Appl. Phys. Lett. **72,** 2963 (1998).
37. O.I. Lebedev, G. Van Tendeloo, S. Amelinckx, H.L. Ju, and K. Krishnan, Philos. Mag. A **80,** 673 (2000).
38. E. Gommert, H. Cerva, A. Rucki, R. von Helmolt, J. Wecker, C. Kuhrt, and K. Samwer, J. Appl. Phys. **81,** 5496 (1997).
39. P. Lu, F. Chu, Q.X. Jia, and T.E. Mitchell, J. Mater. Res. **13,** 2302 (1998).
40. C.J. Lu, Z.L. Wang, C. Kwon, and Q.X. Jia, J. Appl. Phys. (2000, in press).
41. T.-W. Li [private communication, cited in the paper published at Appl. Phys. Lett. **74,** 1615 (1999)].
42. Q. Gan, R.A. Rao, and C.B. Eom, Appl. Phys. Lett. **70,** 1962 (1997).
43. Y. Wu, Y. Suzuki, U. Rüdiger, J. Yu, A.D. Kent, T.K. Nath, and C.B. Eom, Appl. Phys. Lett. **75,** 2295 (1999).